Phys. Status Solidi A **212,** No. 10, 2174–2178 (2015) / **DOI** 10.1002/pssa.201532198

physica status solidi a
www.pss-a.com
applications and materials science

Transparent conductive nanoporous aluminium mesh prepared by electrochemical anodizing

Aliaksandr Hubarevich[1], Mikita Marus[1], Andrei Stsiapanau[2], Aliaksandr Smirnov[2], Junliang Zhao[1], Weijun Fan[1], Hong Wang[*,1], and Xiaowei Sun[,1]**

[1] School of Electrical and Electronic Engineering, Nanyang Technological University, Nanyang Avenue 50, 639798 Singapore, Singapore
[2] Department of Micro- and Nano-Electronics, Belarusian State University of Informatics and Radioelectronics, P. Brovki 6, 220013 Minsk, Belarus

Received 18 March 2015, revised 27 May 2015, accepted 27 May 2015
Published online 22 June 2015

Keywords aluminium, anodizing, liquid crystal cells, porous materials, transparent conductive layers

[*] Corresponding author: e-mail EWANGHONG@ntu.edu.sg, Phone: +65 679 043 58, Fax: +65 679 333 18
[**] e-mail EXWSUN@ntu.edu.sg, Phone: +65 679 053 69, Fax: +65 679 333 18

A non-lithographic method for the fabrication of the transparent conductive nanoporous aluminium (Al) mesh is presented. The electrochemical anodizing of Al layer deposited on the glass substrate was used to obtain the mesh. The average transmittance of 10–60% in 400–800 nm wavelength range and the sheet resistance of 10–1000 $\Omega\,sq^{-1}$ have been obtained for Al mesh with disordered pores arrangement. It was found that transmittance of uniformly arranged porous mesh is increased up to 80–90% with the conductivity range of 25–100 $\Omega\,sq^{-1}$. Our results demonstrate porous Al mesh as a strong candidate of low-cost transparent conductive electrode, especially for flexible electronics.

1 Introduction Rapid increase of indium price leads the search of transparent conductive layers (TCLs) alternative to the indium tin oxide (ITO) [1, 2]. Such TCLs should possess technological parameters similar to ITO: the transmittance more than 80% and the sheet resistance varied from 10 to 100 $\Omega\,sq^{-1}$ [3]. Moreover, alternative TCLs should be preferably flexible and have low cost. Different materials such as carbon nanotubes [4, 5], graphene layers [6, 7], zinc oxides [8], organic polymers [9], ultra thin metallic layers [10, 11] and metallic nanogratings [12–15] were proposed as possible TCL candidates. But so far none of them has been adopted to replace the ITO [4–9]. Thin metallic layers of 10–50 nm thickness are the simplest flexible TCLs which can transmit up to 50% of incoming light in the visible spectrum [16]. Modifying these metallic layers to nanogratings can improve their opto-electronic performance up to that of ITO [14, 17–20]. The fabrication process of nanogratings includes lithography, nanoimprinting, and solution-processing. This paper presents a non-lithographic method of the fabrication of nanoporous Al TCLs. The transparent conductive nanomesh (or nanograting) was made by electrochemical anodizing of Al [21–23]. Experimental results show that mesh transmittance and sheet resistance can be easily controlled by the anodizing time and the voltage applied to the electrochemical cell. The average transmittance of 10–60% in 400–800 nm wavelength range and the sheet resistance of 10–1000 $\Omega\,sq^{-1}$ have been obtained for Al mesh with disordered pores arrangement. It was found that transmittance of uniformly arranged porous mesh is increased up to 80–90% with a conductivity range of 25–100 $\Omega\,sq^{-1}$.

2 Materials and methods The starting sample was the glass substrate with the electron beam that evaporated 250 nm thick Al layer. Ten wt% phosphoric acid (H_3PO_4) was used as the electrolyte in the anodizing process. The electrolyte was frozen to 5 °C to decrease the speed of the anodizing. The potentiostatic regime with voltages of 100 and 180 V was applied to the electrochemical cell. The porous alumina (Al_2O_3) was removed in the mixture of phosphoric acid (6 wt%) and chromic acid (1.8 wt%) at 50 °C for 30 min. The O-ring electrochemical cell with diameter of 1–2 cm and the platinum cathode was used in the experimental setup.

The feasibility of the nanoporous Al mesh for device applications was validated on the liquid crystal cells. The fabrication process of the liquid crystal cell based on twisted nematic effect included the following steps: (i) formation of the bottom Al nanoporous mesh and top ITO electrodes on the glass substrates; (ii) applying of the polyamide; (iii) annealing at 180 °C; (iv) rubbing of the polyamide; (v) deposition of the spacers and sealing of the cell; (vi) injecting of the liquid crystal; and (vii) attaching of the polarisers and final control.

The finite-difference time-domain (FDTD) method is used for the optical property calculation of the hexagonally arranged porous Al mesh. It is available from the commercial software package [24]. The simulation area was cut to the unit cell, where the periodic boundary conditions were applied along x and y directions and the perfectly matched boundary conditions were applied along z direction. The wavelength range of the incoming light was ranged from 300 to 800 nm. The sheet resistance is calculated by the percolation model [25, 26]. According to this model, the sheet resistance of the porous mesh is given by

$$R_{\mathrm{sh}} = \frac{1}{h\sigma_0(\phi_{\mathrm{f}} - \phi_{\mathrm{crit}})^t}, \qquad (1)$$

where σ_0 is the conductivity of the metal, ϕ_{f} is the volume fraction of the patterned metal layer, ϕ_{crit} is the volume fraction threshold when the conductivity of the patterned metal layer is zero, h is the thickness of the metal layer, and t is the critical exponent. The value of the critical exponent is set to 1.75 according to Ref. [26]. For detailed evaluation of ϕ_{f} and ϕ_{crit} for the proposed structure with the hexagonal pore arrangement, see the Supporting Information (online at: www.pss-a.com). The above-mentioned methods were successfully implemented by our team in Ref. [27], where the simulation results were in good agreement with the experimental data.

3 Results and discussion The full technological process of Al nanoporous mesh prepared by the electrochemical anodizing is shown in Fig. 1a. The region 0–t_1 (blue dashed curve in Fig. 1a) is the transformation process of the bulk Al layer to the nanoporous Al_2O_3 and its growth (step 1 in inset of Fig. 1a). This region is well explained in the literature [21–23]. It is worth to mention that Al_2O_3 pores have semi-spherical bottom shape. In result, the porous Al mesh is formed (step 2 in inset of Fig. 1a) when these semi-spherical bottoms reach the glass substrate (at time t_1). The region t_1–t_2 (red solid curve in Fig. 1a) is nanoporous Al mesh formation region. During this period, the pores of Al mesh keep growth (steps 3 and 4 in inset of Fig. 1a) until time t_2 when they are merely connected before mesh broken (step 5 in inset of Fig. 1a). Figure 1b is the close up of Al mesh formation region t_1–t_2.

The duration of this formation region is determined by the etching rate of Al, which can be easily controlled by the

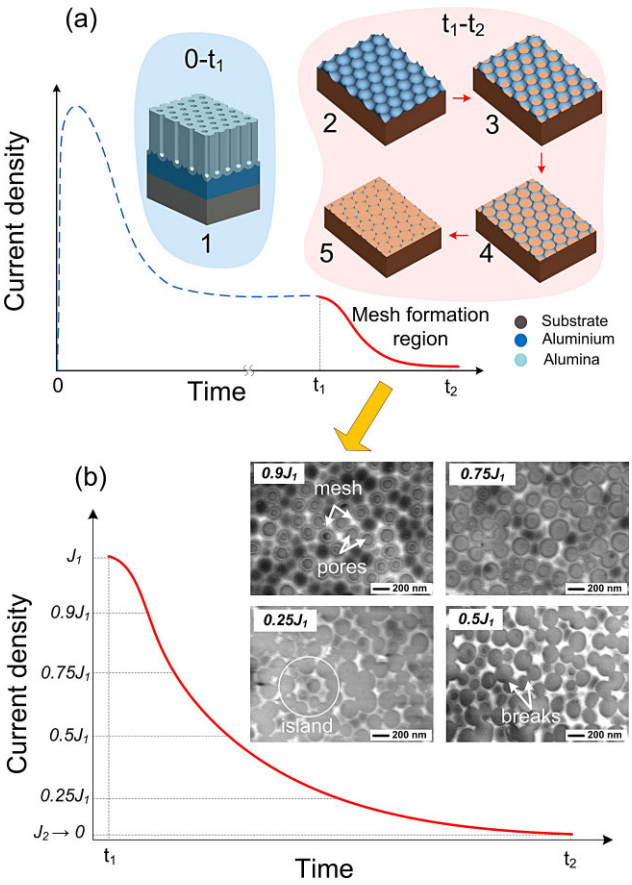

Figure 1 Technological process of nanoporous Al mesh prepared by the electrochemical anodizing: region 0–t_1 is porous Al_2O_3 formation and its growth; region t_1–t_2 is porous Al mesh formation.

solution temperature. We have found that with the solution cooling from room temperature to 5 °C, the etch rate of Al_2O_3 can be reduced by up to 20 times. The corresponding time is about 90–120 s, which is just nice to control the mesh pore size for larger transmission and conductivity. The inset of Fig. 1b demonstrates SEM images of the disordered nanoporous Al mesh obtained by terminating the anodizing at the current density of $0.9J_1$, $0.75J_1$, $0.5J_1$, and $0.25J_1$, where J_1 is the current density at the point t_1. In our case, J_1 was around 0.9 mA cm^{-2}. As can be seen in Fig. 1b, the diameter of pores varies from 120 to 150 nm and from 150 to 180 nm at the current density of $0.9J_1$ and $0.75J_1$, respectively. Further dropping of the current density to $0.5J_1$ increases the diameter of pores to more than 180 nm. The appearance of some breaks is now observed inside mesh or in other words, the mesh becomes disconnected at these places. At the current density of $0.25J_1$, the amount of breaks is increased and the disconnected mesh islands can be seen.

It is obvious that the mesh transmittance and the sheet resistance are both increased when the current density drops from point t_1 to point t_2. Figure 2 shows the correlation between the transmittance and the sheet resistance of the nanoporous Al for the applied voltages of 100 and 180 V at

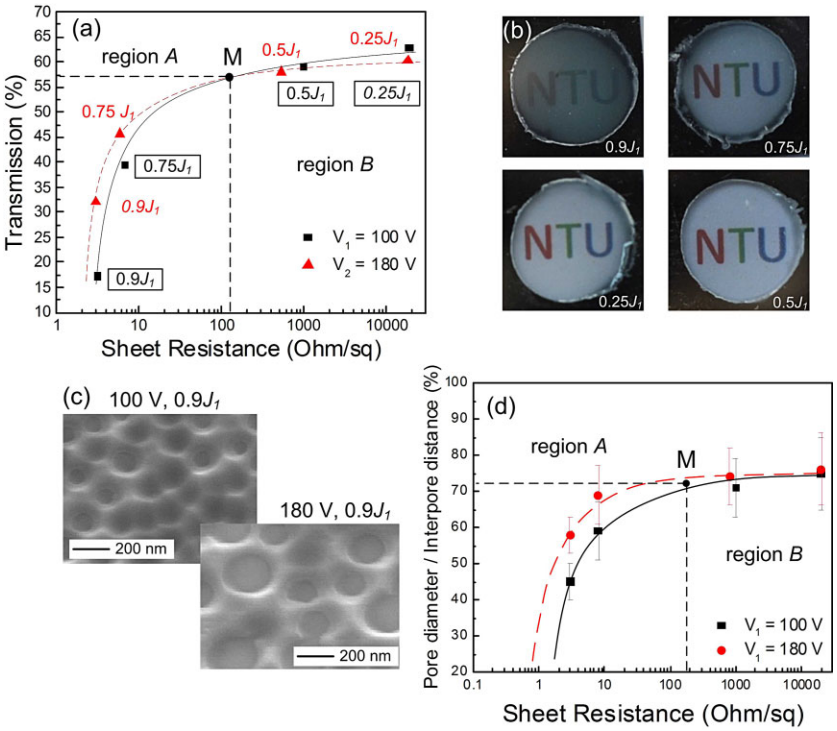

Figure 2 (a) The transmittance versus the sheet resistance of the nanoporous Al mesh obtained by the anodizing at the applied voltage of 100 (black-solid curve) and 180 V (red-dashed curve) and the current densities of $0.9J_1$, $0.75J_1$, $0.5J_1$, and $0.25J_1$. (b) Nanoporous Al mesh of the circle shape and diameter of 1 cm obtained by the anodizing at the applied voltage of 100 V and the current densities of $0.9J_1$, $0.75J_1$, $0.5J_1$, and $0.25J_1$. (c) SEM images of the nanoporous Al mesh obtained by the anodizing at the applied voltages of 100 (left) and 180 V (right) and the current density $0.9J_1$. (d) The ratio of the average pore radius to the interpore distance d/a versus the sheet resistance for the applied voltage of 100 (black-solid curve) and 180 V (red-dashed curve).

the various current densities of $0.9J_1$, $0.75J_1$, $0.5J_1$, and $0.25J_1$. The samples anodized at 100 V with current density of 0.9 and $0.75J_s$ (black solid curve in Fig. 2a) have low sheet resistance of 2 and 10 $\Omega\,sq^{-1}$ and transmittance of 17.5 and 40%, respectively. At the current density of 0.5 and $0.25J_s$, the transmittance was around 60 and 62.5%, while the sheet resistance was significantly increased up to 1000 and 10,000 $\Omega\,sq^{-1}$, respectively. The drastic increase in the resistivity can be explained by the appearance of the mesh breaks and disconnected Al islands during the mesh formation (Fig. 1b). Figure 2b shows the optical images of the circular nanoporous Al meshes with a diameter of 1 cm, which was obtained by the anodizing at the applied voltage of 100 V and the current densities of $0.9J_1$, $0.75J_1$, $0.5J_1$, and $0.25J_1$ mA cm^{-2}. It is seen that the mesh was uniformly anodized for the whole area.

The dashed curve in Fig. 2a demonstrates the dependency of the nanoporous Al mesh transmittance against the sheet resistance at the applied voltage of 180 V and the current densities of $0.9J_1$, $0.75J_1$, $0.5J_1$, and $0.25J_1$. Curiously, the two distinct regions are observed for the solid and dashed curves: the transmittance of the dashed curve is higher at given sheet resistance values before cross-over point *M* (region A), while the opposite behaviour takes place after the point *M* (region B). Such effect can be explained by the difference of the ratio of the pore diameter to the interpore distance *d*/*a* of the nanoporous Al mesh obtained by the anodizing at the applied voltages of 100 and 180 V. It is well-known that higher anodizing voltages create porous Al_2O_3 with larger interpore distances [21]. In our case, the average interpore distance is ~200 and ~275 nm for the nanoporous Al mesh obtained at the applied voltage of 100 and 180 V, respectively (Fig. 2c). The large area SEM images are shown in Fig. S2 of the Supporting Information. Figure 2b illustrates the ratio of the pore diameter to the interpore distance *d*/*a* versus the sheet resistance for the nanoporous Al mesh anodized at 100 and 180 V. It can be seen that *d*/*a* ratio for the red and black curves is far different in the region A. For example, *d*/*a* ratio at the sheet resistance of 2 $\Omega\,sq^{-1}$ is 50 and 25% for *a* equal to 200 and 275 nm, respectively. The opposite case is observed in the region B: the difference of the *d*/*a* ratio for *a* of 200 and 275 nm differs not more than 5%. In result, the *pore size* is the key factor which influences on the mesh transmittance in the region A, while the mesh volume limits the transmittance in the region B.

The formation of the ordered mesh is a way to improve opto-electronic properties by the minimising of the volume of Al mesh breaks and the quantity of disconnected islands. The ordered mesh with the hexagonal pore arrangement could be achieved using the two-step anodizing process [28], pre-imprinting [29], or using self-assembled nanoparticles followed by anodizing [30]. Figure 3a illustrates the dependency of the simulated hexagonal Al nanoporous mesh transmittance as the fraction of the sheet resistance for the interpore distance *a* varied from 100 to 500 nm. The two regions are observed as in the experiments (Fig. 2a): the mesh with the larger interpore distance has higher transmittance and conductivity before the cross-over point *M*; the mesh with the smaller interpore distance has higher both transmittance and sheet resistance after point *M*. It is obvious that these two regions are in good agreement with

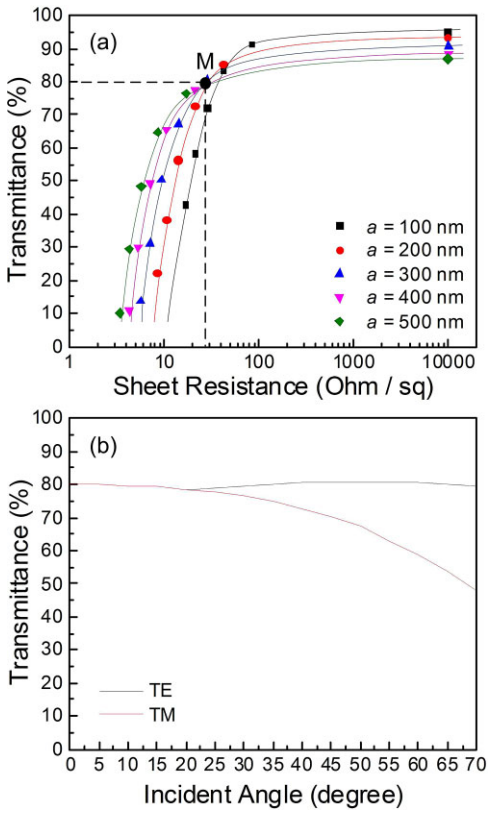

Figure 3 (a) Simulated transmittance of Al mesh versus the sheet resistance. (b) Simulated transmittance of Al mesh versus the incident light angle.

the previous experiments. It is interesting to note that cross-over point M has moved from 100 to 20 $\Omega\,sq^{-1}$ at horizontal axis and up from 57.5 to 80% at vertical axis. In result, the optimal transmittance of 80% with low sheet resistance of 20 $\Omega\,sq^{-1}$ can be realised with the ordered pore arrangement. This is comparable result with the conventional ITO TCLs which can be seen in Fig. S3 in the Supporting Information.

Figure 3b shows the dependence of the incident light angle with the different polarizations calculated based on the design at the cross-over point M. The transmittance keeps almost the constant until 70° for the transverse–electric light polarization, while for the transverse–magnetic light, transmittance starts to demonstrate the dropping after 25° and reaches 50% at 70°, which is explained by the increase of the reflectance [31].

Figure 4 illustrates a working liquid crystal cell based on the twisted nematic effect with area of $2 \times 2\,cm^2$. The Al nanoporous mesh is used as one of the electrodes. The uniform untwist of the liquid crystals results in blocking the transmission of the incoming light when the voltage is applied (ON state). The light is transmitted in the OFF state when the liquid crystals are intrinsically twisted. The result suggests that Al nanoporous mesh could be a good candidate of low-cost transparent conductive electrode.

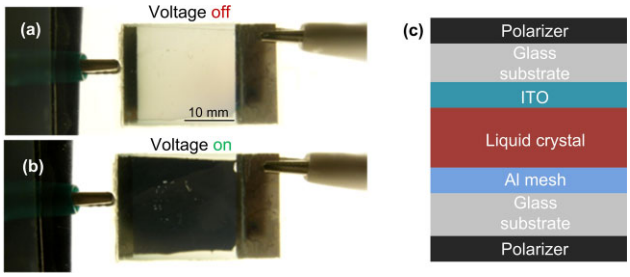

Figure 4 Liquid crystal cell based on twisted nematic effect with top ITO and bottom Al nanoporous electrodes. (a) Liquid crystal cell in the OFF state. (b) Liquid crystal cell in the ON state. (c) Cross-section of the presented liquid crystal cell.

4 Conclusions The porous transparent conductive nanomesh was fabricated by the electrochemical anodizing of Al on the glass substrate. The transmittance and the sheet resistance can be easily controlled by applying different voltages to the electrochemical cell and terminating of the anodizing process at different current densities. The uniform pores arrangement allows to improve the optical and electrical performance up to ITO layers. The average transmittance of 60–80% for 400–800 nm wavelength range and the sheet resistance of 10–100 $\Omega\,sq^{-1}$ were obtained for the samples with the interpore distances of 100–500 nm. This demonstrates the mesh as the potentially transparent conductive layer for various opto-electronic applications, especially for the flexible electronics.

Supporting Information

Additional supporting information may be found in the online version of this article at the publisher's website.

Acknowledgement This project is supported by National Research Foundation of Singapore (No. NRF-CRP11-2012-01).

References

[1] P. C. Vesborg and T.F. Jaramillo, RSC Adv. **2**, 7933 (2012).
[2] F. K. Reiser, C. Rodrigues, and D. Rosa, in: Proc. 5th User Forum Thin-Film Photovoltaics, Würzburg, Germany, 2009, pp. 120–125.
[3] K. Ellmer, Nature Photon. **6**, 809 (2012).
[4] M. Zhang, S. Fang, A. A. Zakhidov, S. B. Lee, A. E. Aliev, C. D. Williams, K. R. Atkinson, and H. Baughman, Science **309**, 1215 (2005).
[5] Z. Wu, Z. Chen, X. Du, J. M. Logan, J. Sippel, M. Nikolou, K. Kamaras, J. R. Reynolds, D. B. Tanner, A. F. Hebard, and A. G. Rinzler, Science **305**, 1273 (2004).
[6] J. Wu, M. Agrawal, H. A. Becerril, Z. Bao, Z. Liu, Y. Chen, and P. Peumans, ACS Nano **4**, 43 (2009).
[7] M. Cox, A. Gorodetsky, B. Kim, K. S. Kim, Z. Jia, P. Kim, C. Nuckolls, and I. Kymissis, Appl. Phys. Lett. **98**, 123303 (2011).
[8] Z. L. Wang, J. Phys.: Condens. Matter **16**, R829 (2004).
[9] A. G. MacDiarmid, Synth. Met. **125**, 11 (2001).
[10] B. O'Connor, C. Haughn, K.-H. An, K. P. Pipe, and M. Shtein, Appl. Phys. Lett. **93**, 223304 (2008).

[11] D. Ghosh, L. Martinez, S. Giurgola, P. Vergani, and V. Pruneri, Opt. Lett. **34**, 325 (2009).
[12] M. G. Kang, T. Xu, H. J. Park, X. Luo, and L. J. Guo, Adv. Mater. **22**, 4378 (2010).
[13] H. Wu, L. Hu, M. W. Rowell, D. Kong, J. J. Cha, J. R. McDonough, J. Zhu, Y. Yang, M. D. McGehee, and Y. Cui, Nano Lett. **10**, 4242 (2010).
[14] J.-Y. Lee, S. T. Connor, Y. Cui, and P. Peumans, Nano Lett. **8**, 689 (2008).
[15] P. Kuang, J.-M. Park, W. Leung, R. C. Mahadevapuram, K. S. Nalwa, T.-G. Kim, S. Chaudhary, K.-M. Ho, and K. Constant, Adv. Mater. **23**, 2469 (2011).
[16] B. O'Connor, C. Haughn, K.-H. An, K. P. Pipe, and M. Shtein, Appl. Phys. Lett. **93**, 223304 (2008).
[17] L. Hu, H. Wu, and Y. Cui, MRS Bull. **36**, 760 (2011).
[18] M.-G. Kang and L.J. Guo, J. Vac. Sci. Technol. B **26**, 2421 (2008).
[19] J. Shang, H. Qi, H. Feng, L. Wang, J. Zhang, Y. Wang, W. Hao, and T. Wang, Phys. Status Solidi RRL **7**, 1071 (2013).
[20] T. Ackermann, S. Sahakalkan, I. Kolaric, E. Westkämper, and S. Roth, Phys. Status Solidi RRL **9**, 141 (2015).
[21] A. P. Li, F. Müller, A. Birner, K. Nielsch, and U. Gösele, J. Appl. Phys. **84**, 6023 (1998).
[22] S. Z. Chu, K. Wadaa, S. Inouea, M. Isogaib, Y. Katsutab, and A. Yasumori, J. Electrochem. Soc. **153**, B384 (2006).
[23] M. H. Lee, N. Lim, D. J. Ruebusch, A. Jamshidi, R. Kapadia, R. Lee, T. J. Seok, K. Takei, K. Y. Cho, Z. Fan, H. Jang, M. Wu, G. Cho, and A. Javey, Nano Lett. **11**, 3425 (2011).
[24] Lumerical FDTD Solutions. Available from: https://www.lumerical.com/tcad-products/fdtd/.
[25] T. H. Reilly, R. C. Tenent, T. M. Barnes, K. L. Rowlen, and J. Lagemaat, ACS Nano **4**, 615 (2010).
[26] M. Weber, and M.R. Kamal, Polym. Compos. **18**, 711 (1997).
[27] M. Marus, A. Hubarevich, H. Wang, A. Smirnov, X. W. Sun, and W. Fan, Opt. Express **23**, 6209 (2015).
[28] S. Ono, M. Saito, M. Ishiguro, and H. Asoh, J. Electrochem. Soc. **151**, B473 (2004).
[29] K. Yasui, K. Nishio, H. Nunokawa, and H. Masuda, J. Vac. Sci. Technol. B **23**, L9 (2005).
[30] T. Nakanishi, E. Tsutsumi, K. Masunaga, A. Fujimoto, and K. Asakawa, Appl. Phys Express **4**, 025201 (2011).
[31] R. Gordon, Phys. Rev. B **75**, 193401 (2007).

